ACS SENSORS

pubs.acs.org/acssensors Article

An Activity-Based Nanosensor for Traumatic Brain Injury

Julia A. Kudryashev, Lauren E. Waggoner, Hope T. Leng, Nicholas H. Mininni, and Ester J. Kwon*

Cite This: https://dx.doi.org/10.1021/acssensors.9b01812 Read Online

ACCESS | Metrics & More | Article Recommendations | Supporting Information

ABSTRACT: Currently, traumatic brain injury (TBI) is detected by medical imaging; however, medical imaging requires expensive capital equipment, is time- and resource-intensive, and is poor at predicting patient prognosis. To date, direct measurement of elevated protease activity has yet to be utilized to detect TBI. In this work, we engineered an activity-based nanosensor for TBI (TBI-ABN) that responds to increased protease activity initiated after brain injury. We establish that a calcium-sensitive protease, calpain-1, is active in the injured brain hours within injury. We then optimize the molecular weight of a nanoscale polymeric carrier to infiltrate into the injured brain tissue with minimal renal filtration. A calpain-1 substrate that generates a fluorescent signal upon cleavage was attached to this nanoscale polymeric carrier to generate an engineered TBI-ABN. When applied intravenously to a mouse model of TBI, our engineered sensor is observed to locally activate in the injured brain tissue. This TBI-ABN is the first demonstration of a sensor that responds to protease activity to detect TBI.

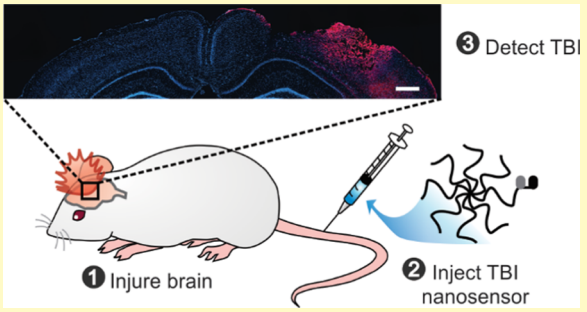

KEYWORDS: *traumatic brain injury, activity-based nanosensor, nanomedicine, calpain-1, protease activity*

Traumatic brain injury (TBI) affects over 2.8 million people annually in the United States and leads to the hospitalization of ∼300 000 patients per year.[1] Among TBI patients who require surgical intervention, there is a 50% lower mortality rate and decreased length of stay if they receive surgery within 4 h of hospital admission,[2] indicating the importance of rapid diagnosis and triage to improve outcomes. However, current diagnosis is achieved by medical imaging, typically computed tomography (CT) and magnetic resonance imaging (MRI), both of which are time- and resource-intensive and have a limited ability to predict patient prognosis.[3] Moreover, while medical imaging can identify macroscopic structural deformations in the brain, it currently does not yield information on the destructive biological activity that may unfold after injury. This secondary injury, which may include sustained protease activity, inflammation, excitotoxicity, and neuronal death, begins immediately after the primary injury and may lead to chronic neurodegeneration and a poorer patient prognosis.[4] Thus, a diagnostic that yields information on biological activity may inform improved clinical care.

Breakdown products shed into the blood and cerebrospinal fluid have been recently investigated as biomarkers to detect pathological processes in TBI.[5] These breakdown products originate from the degradation of nervous tissue as part of a prolonged secondary injury that begins within minutes after TBI.[6] To date, there is only one TBI biomarker-based diagnostic on the market; it is based on two separate enzyme-linked immunosorbent assays (ELISAs) to measure serum levels of the breakdown products glial fibrillary acidic protein (GFAP) and ubiquitin C-terminal hydrolase L1 (UCH-L1).[7] However, measurement of these biomarkers relies on the generation, stability, and transport of these byproducts;[8] direct measurement of degradative activity may be more representative of disease and therefore provide information that is more actionable for intervention. Calpain-1, a calcium-dependent protease expressed in neurons, glia, and endothelial cells within the brain, undergoes sustained activation after TBI due to pathological elevations of intracellular calcium.[6,9,10] Calpain-1 activity generates many breakdown products that are currently under investigation as biomarkers for TBI, including myelin basic protein, neurofilaments, and αII-spectrin.[5] Calpain-1 inhibition has been under investigation as a treatment for TBI,[11] and its byproducts can potentially predict patient prognosis after mild and severe TBI,[12,13] highlighting the importance of calpain-1 in the injury sequelae and its prognostic potential. Thus, the detection of calpain-1 protease activity is a promising candidate for TBI diagnosis.

To explore the potential of activity-based sensors to detect TBI, our goal was to engineer a vascularly administered sensor that can accumulate in the injured brain tissue and produce a

Received: September 16, 2019
Accepted: February 26, 2020
Published: February 26, 2020

https://dx.doi.org/10.1021/acssensors.9b01812
ACS Sens. XXXX, XXX, XXX−XXX

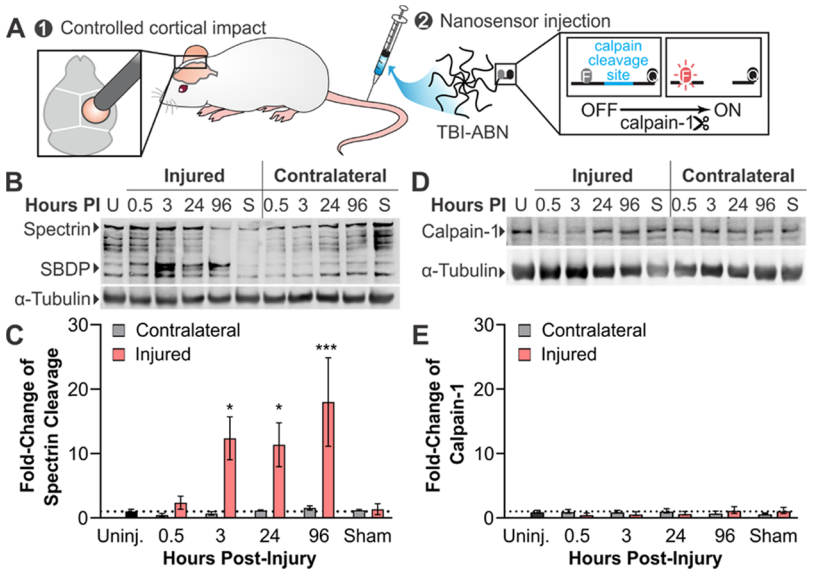

Figure 1. Design of a TBI activity-based nanosensor. (A) Overview of TBI-ABN design. (B) Time course post injury (PI) of αII-spectrin cleavage in controlled cortical impact (CCI)-injured cortices. (C) Quantification of calpain-1-specific 145 and 150 kDa αII-spectrin breakdown products (SBDP), normalized to α-tubulin and untreated control (n = 3, mean ± standard error (SE), *p < 0.05, ***p < 0.001, two-way analysis of variance (ANOVA), and Dunnett's post hoc test against uninjured control). (D) Time course and (E) quantification of 80 kDa calpain-1 denoted by the arrow, normalized to α-tubulin and untreated control (n = 3, mean ± SE). Uninjured (U) mice received no surgery. Sham (S) mice received a craniotomy and no injury.

signal in response to calpain-1 activity (Figure 1A). A similar activity-based sensor strategy has been demonstrated for the sensitive detection of cancer and liver fibrosis in previous works,[14,15] but has yet to be applied to any brain disorders. First, we established increased calpain-1 activity that is independent of calpain-1 expression levels in the first few hours after TBI in mice, validating the need for a sensor of enzyme activity rather than enzyme levels. To engineer a diagnostic that can be delivered into the vasculature, we exploit the size-dependent accumulation of nanoscale polymeric carriers into the site of injury, where the blood−brain barrier (BBB) is compromised and allows extravasation of nanoscale materials. To detect calpain-1 activity, we engineered a fluorescent resonance energy-transfer (FRET) peptide, which activates in the presence of active calpain-1. Combining the peptide and carrier, we engineered a TBI activity-based nanosensor (TBI-ABN). This TBI-ABN activates at the site of injury in a mouse model of brain injury after intravenous administration. To our knowledge, TBI-ABN is the first demonstration of an activity-based sensor for TBI.

EXPERIMENTAL SECTION

Synthesis of Poly(ethylene glycol) (PEG) Conjugates. Calpain substrate peptide (QSY21-QEVYGAMP-K(Cy5)-PEG2-GC-NH2) was synthesized by CPC Scientific Inc. (Sunnyvale, CA). PEG2 stands for poly(ethylene glycol). 8-arm PEG amine and PEG maleimide (tripentaerythritol) were purchased from Jenkem Technology (Beijing, China). PEG amine was reacted with 1 mol equivalent of VivoTag-S 750 (PerkinElmer, Boston, MA). PEG maleimide was reacted with 1, 2, and 4 mol equivalences of the peptide in the presence of 50 mM triethylamine (TEA) and quenched with an excess of L-cysteine. All conjugates were dialyzed in water, and the final concentrations were determined by absorbance of VivoTag or Cy5 using a Spark multimode microplate reader (Tecan Trading AG, Switzerland). The L-cysteine PEG maleimide control was dissolved by weight. Hydrodynamic diameters of unconjugated PEG amine were measured via dynamic light scattering (DLS) with a Zetasizer Nano (Malvern Panalytical).

In Vitro Reaction Kinetics Assay. Free peptide and conjugates were incubated with 26.6 nM recombinant human calpain-1 (Sigma-Aldrich) in 50 mM *N*-(2-hydroxyethyl)piperazine-*N*′-ethanesulfonic acid (HEPES), 50 mM NaCl, 2 mM ethylenediaminetetraacetic acid (EDTA), 5 mM $CaCl_2$, 5 mM β-mercaptoethanol, 10% mouse plasma in phosphate-buffered saline (PBS), or 13.5 nM human α-thrombin (Haematologic Technologies) in TCNB buffer. Mouse plasma was prepared by centrifuging blood collected with EDTA. Fluorescence readings were taken every 90 s at 37 °C for 1 h. Reaction curves were normalized to controls, and their initial velocities were fitted to a Michaelis−Menten curve in GraphPad Prism (8.1.2).

Controlled Cortical Impact (CCI) Mouse Model of TBI. All mouse protocols were approved by the University of California San Diego's Institutional Animal Care and Use Committee (IACUC). Female C57BL/6J mice of 8−12 weeks old (Jackson Labs) were used for all experiments. Mice were anesthetized with 2.5% isoflurane, and the head was secured in a stereotaxic frame. A midline incision was made to expose the skull, and a 4 mm diameter craniotomy was performed over the right hemisphere between bregma and lambda. The controlled cortical impact was applied to the exposed dura of the cortex with the ImpactOne (Leica Biosystems) fitted with a stainless steel 2 mm diameter probe at a velocity of 3 m/s and a 2 mm depth.

Biodistribution and In Vivo Sensor Activation. Two hours after CCI, 2 nmol of VivoTag-PEG in 100 μL PBS (n = 4 each for biodistribution) or 8 nmol of TBI-ABN in 100 μL PBS (n = 6 for sensor activation analysis) were intravenously administered via the tail vein. Control mice received the same volume of PBS. Two hours after administration, mice were transcardially perfused with USP saline followed by 10% formalin. Fluorescence was measured with an Odyssey scanner (Li-Cor Biosciences) on the same day as collection. The mean fluorescence intensity per area was analyzed using ImageJ.

Immunohistochemistry and Sensor Quantification in Brain Tissue Slices. Organs were fixed with 10% formalin solution at 4 °C overnight, equilibrated in 30% w/v sucrose, and frozen in OCT (Tissue-Tek). Coronal tissue slices 10 μm thick were stained using conventional protocols. The following primary antibodies were used: 1:200 calpain-1 (Abcam, ab108400) and 1:200 CD31 (BD, 553370). Sensor activation was quantified in three tissue slices per brain up to 1.5 mm caudal from the center of the injury. Cy5 signal in each slice extending 1.5 mm down from the top of the cortex was averaged

https://dx.doi.org/10.1021/acssensors.9b01812
ACS Sens. XXXX, XXX, XXX−XXX

between slices from each brain and then normalized to the signal from uninjured PBS controls using ImageJ. Images were captured with a Nikon Eclipse Ti2 microscope fitted with a Hamamatsu Orca-Flash 4.0 digital camera.

Protein Analysis. At the designated time points after injury, injured and contralateral cortices were harvested and immediately frozen. Sham injured mice received a craniotomy and no injury, and the tissue was harvested 3 h after surgery. Western blots were performed following conventional protocols. The following primary antibodies were used: 1:2000 αII-spectrin (Abcam, ab11755), 1:1000 calpain-1 (Abcam, ab108400), or 1:5000 α-tubulin (Cell Signaling, 3873). Membranes were imaged on a Li-Cor Odyssey scanner, and densitometric analysis of the Western blots was done in ImageJ.

Software and Statistics. All data were analyzed in GraphPad Prism (8.1.2). All post hoc tests were conducted with $p < 0.05$ to identify statistical significance between samples. All images were analyzed with ImageJ (1.52p).

RESULTS AND DISCUSSION

Calpain-1 Locally Activates in a Mouse Model of TBI. We first established the levels of calpain-1 activity and protein in a mouse model of TBI. The controlled cortical impact (CCI) model of TBI is a reproducible and well-characterized method to create a localized injury in the brain.[16−18] To assess calpain-1 activity, 150 and 145 kDa breakdown products of the native calpain-1 substrate αII-spectrin were measured, as described previously.[19] These spectrin breakdown products (SBDPs) were shown to increase to greater than 10-fold in the injured hemisphere at 3 h post injury compared to that in the uninjured brains (Figure 1B,C). This increase was sustained up to 96 h post injury. By contrast, the uninjured, contralateral hemisphere did not show a significant elevation of SBDPs. A sham control group that underwent a craniotomy but no injury exhibited similar levels of SBDPs to uninjured mice, confirming that spectrin proteolysis was the result of a direct impact to the brain tissue and not the surgical procedures. We thus establish that calpain-1 activity is increased after CCI and activity is localized to the injured hemisphere, consistent with the previously reported rodent models of CCI.[17,19−21]

To determine that increased spectrin cleavage was due to increased activity of calpain-1 and not increased levels of calpain-1, calpain-1 protein levels were also measured. No significant changes were observed in the protein levels of the 80 kDa large subunit of calpain-1 between injured and uninjured brains (Figure 1D,E). Furthermore, assessment of calpain-1 via immunohistochemistry of brain slices showed only a local increase in calpain-1 detected 4 h post injury in the immediate injury area, whereas calpain-1 levels appeared to be unchanged in the uninjured cortex and the greater injury periphery when compared to those in the uninjured brains (Figure S1). These results indicate that the observed increase in αII-spectrin proteolysis (Figure 1B) is likely due to increased calpain-1 activity and not increased calpain-1 expression. Previous studies have shown that calpain-1 expression can be increased after injury, but its elevation is delayed by ∼24 h.[22] Therefore, a sensor to detect calpain-1 activity may be effective in the first few hours after TBI.

Large-Molecular-Weight Polymeric Carriers Accumulate in the Site of Injury after CCI. We next focused on a nanoscale delivery carrier for our nanosensor. Shortly after TBI, the vasculature at the site of injury is compromised due to the mechanical damage followed by dysregulation of the neurovascular unit.[23,24] This pathological hallmark of TBI allows for the delivery of nanoscale cargo to the brain within the first 24 h after injury, similar to the enhanced permeability and retention (EPR) effect described for nanoparticles in tumors.[25] On their own, small peptides have a short circulation half-life in vivo due to renal clearance and proteolytic degradation in the bloodstream. We hypothesized that blood circulation time and subsequent tissue retention of the peptide would increase through its conjugation to a larger, neutrally charged, and minimally immunogenic polymeric carrier such as poly(ethylene glycol) (PEG).[26] While studies have been done on the biodistribution of rigid nanoparticles, including PEGylated polystyrene nanoparticles and liposomes after TBI,[27,28] and polystyrene nanoparticles after microdialysis probe insertion,[29] there has not yet been a study into the distribution of PEG after TBI. To maximize the delivery of the TBI nanosensor through the compromised BBB after injury, we evaluated how the molecular weight of 8-arm PEG affects its accumulation into the injured tissue after CCI injury. 8-arm PEG was chosen as the carrier because it allows for the possibility of multiplexing through the conjugation of ligands to each individual arm. PEG carriers (10, 20, and 40 kDa) were evaluated for distribution into major organs after intravenous injection 2 h after CCI in mice (Figures 2A and S2). This timeline was chosen to be within the initial 4 h of secondary injury after CCI when a quick diagnosis and intervention of calpain are critical.[17] The highest accumulation for 10 kDa PEG was seen in the kidneys with little accumulation in the brain, whereas the 20 and 40 kDa PEGs had significant accumulation in the injured brain and significantly less accumulation in the kidneys compared to the 10 kDa PEG. In the brain, 20 and 40 kDa PEGs accumulated significantly more in the injured hemisphere than in the contralateral hemisphere by approximately 7- and 5-fold, respectively

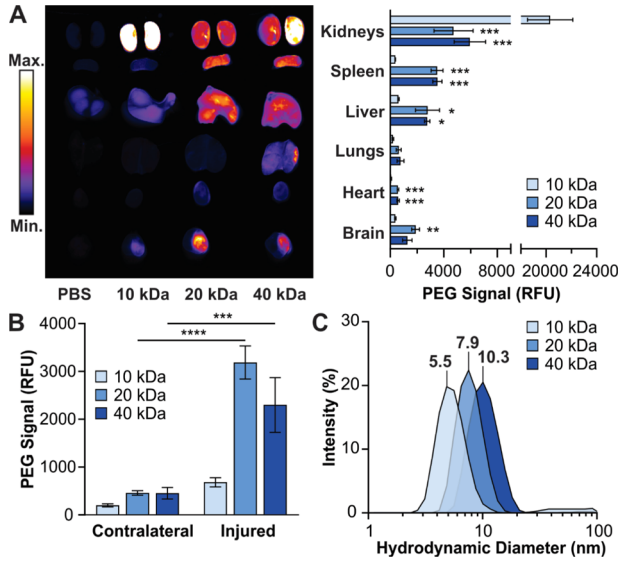

Figure 2. Large-molecular-weight PEG carriers localize to the region of injury in a mouse model of TBI. (A) Fluorescence image of major organs after intravenous injection of fluorescently labeled PEG of various sizes (left) was quantified and the signal was normalized to PBS-injected animals (right) ($n = 4$, mean ± SE, $^{*}p < 0.05$, $^{**}p < 0.01$, $^{****}p < 0.001$, ordinary one-way ANOVA, and Tukey's post hoc test compared within each organ). (B) PEG distribution in injured or contralateral brain hemispheres ($n = 4$, mean ± SE, $^{***}p < 0.001$, $^{****}p < 0.0001$, two-way ANOVA, and Sidak's post hoc test within each size). (C) Size distribution of 10, 20, and 40 kDa PEGs.

https://dx.doi.org/10.1021/acssensors.9b01812
ACS Sens. XXXX, XXX, XXX−XXX

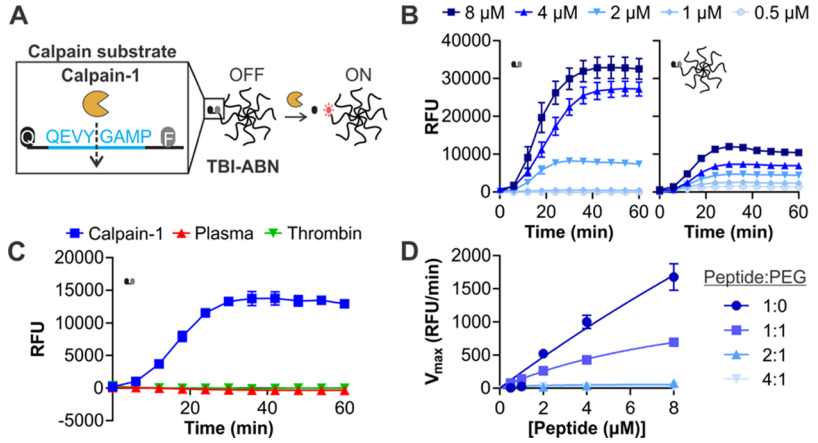

Figure 3. Calpain substrate is cleaved by calpain-1 as free peptide and when conjugated to PEG carrier. (A) Schematic of calpain substrate peptide, conjugated to 8-arm PEG to form TBI-ABN (Q = quencher, F = fluorophore). (B) Cleavage of free peptide (left) and 1:1 peptide:PEG (right) with recombinant human calpain-1 (n = 3, mean ± SD). (C) Cleavage of 8 μM peptide with recombinant human calpain-1, mouse plasma, or human α-thrombin (n = 3, mean ± SD). (D) Michaelis–Menten reaction kinetics of peptide:PEG ratios of 1:0, 1:1, 2:1, and 4:1 calpain-1 cleavages (n = 3, mean ± SD).

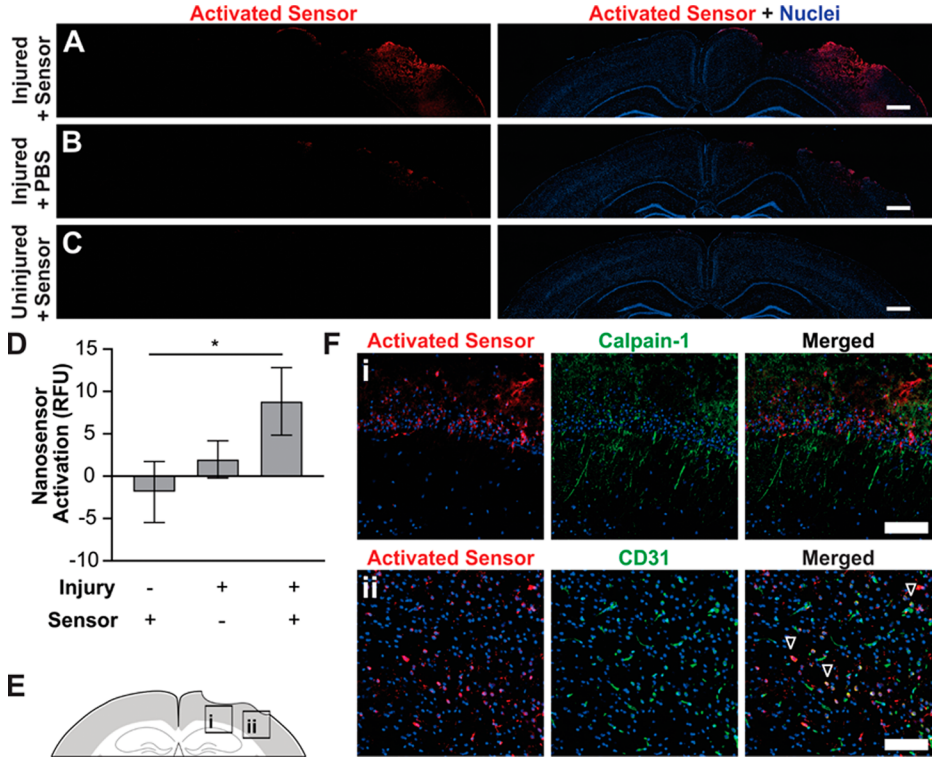

Figure 4. Calpain sensor activates in the injured brain tissue after intravenous delivery. (A–C) Representative coronal brain slices from injured and uninjured brains (blue, nuclei; red, activated nanosensor; scale bar = 500 μm). (D) Quantification of mean sensor intensity in the injured hemisphere normalized to uninjured control brains (n = 6, mean ± SE, *p = 0.0851, ordinary one-way ANOVA, and Sidak's post hoc test). (E) Map and (F) insets from slices adjacent to (A), showing sensor localization relative to (i) calpain-1 and (ii) CD31 in the injury periphery (blue, nuclei; red, activated nanosensor; green, calpain-1 (top) or CD31 (bottom); outlined arrows, overlap of sensor with CD31; scale bar = 100 μm).

(Figure 2B). The hydrodynamic diameters of each carrier in PBS were measured to be 5.57, 7.89, and 10.25 nm for 10, 20, and 40 kDa PEGs, respectively (Figure 2C). The 10 kDa PEG is near the ∼5 nm limit for renal filtration,[30,31] which is reflected in its significant accumulation into the kidneys compared to the 20 and 40 kDa sizes. All three carriers are smaller than the 500 nm size range of materials which have been observed to extravasate into the injured tissue following TBI.[28,32] Thus, 8-arm PEG polymer carriers greater than 20 kDa in size can accumulate in the injured brain.

Calpain Substrate Responds to Calpain-1 Activity. To detect calpain-1 activity, we synthesized a calpain-1-responsive peptide composed of the FRET pair Cy5 and QSY21 separated by a calpain-1-specific cleavage sequence (QEVYGAMP) taken from the native mouse αII-spectrin sequence (Figure 3A).[33] To measure kinetics of cleavage by calpain-1, several concentrations of peptide were incubated with recombinant calpain-1 enzyme in vitro, and peptide cleavage was measured by dequenched Cy5 fluorescence (Figure 3B). Because blood cleavage is a major concern for a sensor administered

https://dx.doi.org/10.1021/acssensors.9b01812
ACS Sens. XXXX, XXX, XXX–XXX

intravenously, nonspecific cleavage of our peptide by blood components was examined by incubation with mouse plasma or human α-thrombin. No significant cleavage of our substrate was observed (Figure 3C). This peptide was then conjugated to 40 kDa 8-arm PEG to increase its circulation time and retention in the injured brain tissue when applied in vivo (Figure 2). The 40 kDa PEG was used over 20 kDa PEG to increase solubility of the peptide, as precipitates were observed with 20 kDa conjugates. Multiple ratios of peptide:PEG were assessed via the same in vitro kinetics assay to optimize for sensor signal in response to calpain-1. It was observed that the conjugation of the peptide:PEG in a 1:1 stoichiometric ratio led to a decrease in the fluorescent signal (Figure 3B) as well as maximum cleavage velocity (Figure 3D) compared to that of the free peptide. For example, the maximum cleavage velocity of the peptide at an 8 μM concentration decreased from 1677.5 to 692.1 RFU/min with conjugation. This decrease was not observed with the peptide in the presence of free unconjugated PEG (Figure S3), suggesting that the direct conjugation of the peptide to PEG impacts peptide cleavage by calpain-1. The addition of multiple peptides:PEG in 2:1 and 4:1 conjugates led to further decreased cleavage velocities compared to that of 1:1 conjugate or free peptide (Figure 3D). Conjugates of 8:1 peptide:PEG precipitated out of solution, suggesting that the increased local concentration of peptides created by physical linkage to a polymeric carrier leads to a decrease in solubility. Due to the benefits of brain accumulation afforded by the PEG, a 1:1 stoichiometric ratio of the peptide and PEG carrier was further evaluated in animal models of TBI.

TBI-ABN Activates in Injured Brain Tissue after CCI. Finally, we tested the activation of the TBI nanosensor in a mouse model of TBI. We have established that calpain-1 has an increased activity independent of expression after brain injury, PEG greater than 20 kDa in molecular weight can accumulate in the injury site, and a FRET peptide substrate is cleaved by calpain-1. Extracellular release of calpain-1 and its substrates by necrotic neurons after injury has been observed in previous studies;[5,34] we therefore expect the activation of our nanosensor without the need for cell internalization. Both increased calpain-1 activity and intravenous access to the brain occur within the same 4 h time scale post injury, so we expect that our TBI-ABN can localize and activate in the injured brain. We note that the diagnosis of TBI within this 4 h window has been demonstrated to be crucial to decrease patient morbidity.[2]

Mice were intravenously injected with sensor 2 h after CCI injury and evaluated for sensor activation 2 h after injection. In the first hours after CCI, focal neurodegeneration has been previously shown to extend from the injury site down to the hippocampus;[17] based on these observations, the top 1.5 mm of coronal brain slices was analyzed for sensor activation after fluorescent imaging. The sensor showed significant activation in the injured brain hemisphere with a higher activated sensor signal compared to the background signal from both injured and uninjured brains (Figure 4A−C). There was minimal activation of the sensor in uninjured brains, likely due to unchanged calpain-1 activity (Figure 1B) and intact BBB. Additionally, there was little difference in signal in uninjured brains and the contralateral hemisphere of injured brains (Figures 4D and S4). These results provide evidence that the sensor produces a signal in response to injury.

We additionally investigated the cellular distribution of sensor activation. Since the TBI-ABN was delivered through an intravenous injection, we assessed TBI-ABN activation in relation to the vasculature by staining for calpain-1 and the endothelial marker, CD31. In the injury periphery, activated TBI-ABN signal was found in proximity to calpain-1 and some signal was also positively stained for endothelial cells (Figure 4E,F). Signal was also detected in the hippocampal CA1 region and dentate gyrus (Figure S5), regions that are identified as sites of extravasation and neurodegeneration following CCI.[18,24] Neurons, glia, and endothelial cells populating these regions are known to experience calcium influxes and abnormal calpain activation following injury[6,9] and are therefore potential sources for TBI-ABN signal.

CONCLUSIONS

We engineered a TBI activity-based nanosensor, TBI-ABN, which responds to calpain-1 activity, accumulates in the injured brain tissue, and activates in a mouse model of brain injury. To our knowledge, our engineered TBI-ABN is the first sensor to detect enzyme activity in TBI and is a proof-of-concept for the development of future activity-based diagnostics for TBI. Activity-based sensors are gaining significance for their ability to be engineered in response to specific biological stimuli, allowing for the capture of pathological processes that cannot be detected by conventional molecular quantification methods.[35] There are notable examples of activity-based sensors in cancer: fluorescently activated polymers can identify tumor margins during surgical resection,[36,37] and urinary sensors can detect and stratify tumors.[14,15,38] Based on these advances in cancer, measuring protease activity with an activity-based sensor to diagnose TBI is a promising strategy.

Now that we have established that a vascularly delivered sensor can activate in brain injury in response to protease activity, in future work, the TBI-ABN will be engineered to release biomarkers for minimally invasive blood-based detection. Signal specificity can be increased by multiplexing substrates for the detection of proteases such as MMP-9, which has local increases in activity following TBI and contributes to BBB breakdown.[39] To further enhance sensitivity and increase tissue accumulation and retention, we can add active targeting ligands, for example, peptides that bind extracellular matrix components exposed after injury.[40−42] In the long term, TBI-ABN can be paired with inhibitors of protease activity, such as small molecule inhibitors of calpain-1,[11] to create nanotheranostics that can detect and treat TBI.

ASSOCIATED CONTENT

Supporting Information

The Supporting Information is available free of charge at https://pubs.acs.org/doi/10.1021/acssensors.9b01812.

Calpain-1 distribution in brain slices 4 hours post injury within injured and uninjured brain tissues; fluorescence images of all organs analyzed for biodistribution; kinetics conjugation control; quantification of mean sensor intensity in the contralateral hemisphere normalized to uninjured control brains; and sensor localization in areas of extravasation (PDF)

https://dx.doi.org/10.1021/acssensors.9b01812
ACS Sens. XXXX, XXX, XXX−XXX

AUTHOR INFORMATION

Corresponding Author

Ester J. Kwon − *Department of Bioengineering, University of California, San Diego, La Jolla, California 92093, United States;* orcid.org/0000-0002-6335-9681; Email: ejkwon@ucsd.edu

Authors

Julia A. Kudryashev − *Department of Bioengineering, University of California, San Diego, La Jolla, California 92093, United States;* orcid.org/0000-0003-3022-0058

Lauren E. Waggoner − *Department of Nanoengineering, University of California, San Diego, La Jolla, California 92093, United States*

Hope T. Leng − *Department of Bioengineering, University of California, San Diego, La Jolla, California 92093, United States*

Nicholas H. Mininni − *Department of Bioengineering, University of California, San Diego, La Jolla, California 92093, United States*

Complete contact information is available at: https://pubs.acs.org/10.1021/acssensors.9b01812

Author Contributions

J.A.K. and E.J.K.: project conceptualization, experimental design, data acquisition and analysis, manuscript preparation; L.E.W.: experimental design, data acquisition; H.T.L. and N.H.M.: data acquisition. All authors have given approval to the final version of the manuscript.

Funding

J.A.K. is supported by the National Science Foundation (NSF) Graduate Research Fellowship Program under Grant No. DGE-1650112. Any opinions, findings, and conclusions or recommendations expressed in this material are those of the authors and do not necessarily reflect the views of the NSF.

Notes

The authors declare no competing financial interest.

ABBREVIATIONS USED

ABN, activity-based nanosensor; BBB, blood−brain barrier; CCI, controlled cortical impact; DLS, dynamic light scattering; TBI, traumatic brain injury

REFERENCES

(1) CDC. *Surveillance Report of Traumatic Brain Injury-Related Emergency Department Visits, Hospitalizations, and Deaths—United States, 2014*, 2019.

(2) Kim, Y. J. The Impact of Time from ED Arrival to Surgery on Mortality and Hospital Length of Stay in Patients With Traumatic Brain Injury. *J. Emerg. Nurs.* **2011**, *37*, 328−333.

(3) Hofman, P. A. M.; Stapert, S. Z.; van Kroonenburgh, M. J. P. G.; Jolles, J.; de Kruijk, J.; Wilmink, J. T. MR Imaging, Single-Photon Emission CT, and Neurocognitive Performance after Mild Traumatic Brain Injury. *Am. J. Neuroradiol.* **2001**, *22*, 441−449.

(4) Maas, A. I. R.; Stocchetti, N.; Bullock, R. Moderate and Severe Traumatic Brain Injury in Adults. *Lancet Neurol.* **2008**, *7*, 728−741.

(5) Wang, K. K.; Yang, Z.; Zhu, T.; Shi, Y.; Rubenstein, R.; Tyndall, J. A.; Manley, G. T. An Update on Diagnostic and Prognostic Biomarkers for Traumatic Brain Injury. *Expert Rev. Mol. Diagn.* **2018**, *18*, 165−180.

(6) Andriessen, T. M. J. C.; Jacobs, B.; Vos, P. E. Clinical Characteristics and Pathophysiological Mechanisms of Focal and Diffuse Traumatic Brain Injury. *J. Cell. Mol. Med.* **2010**, *14*, 2381−2392.

(7) Bazarian, J. J.; Biberthaler, P.; Welch, R. D.; Lewis, L. M.; Barzo, P.; Bogner-Flatz, V.; Gunnar Brolinson, P.; Büki, A.; Chen, J. Y.; Christenson, R. H.; et al. Serum GFAP and UCH-L1 for Prediction of Absence of Intracranial Injuries on Head CT (ALERT-TBI): A Multicentre Observational Study. *Lancet Neurol.* **2018**, *17*, 782−789.

(8) Hori, S. S.; Gambhir, S. S. Mathematical Model Identifies Blood Biomarker-Based Early Cancer Detection Strategies and Limitations. *Sci. Transl. Med.* **2011**, *3*, No. 109ra116.

(9) Czogalla, A.; Sikorski, A. F. Spectrin and Calpain: A "target" and a "Sniper" in the Pathology of Neuronal Cells. *Cell. Mol. Life Sci.* **2005**, *62*, 1913−1924.

(10) Hamakubo, T.; Kannagi, R.; Murachi, T.; Matus, A. Distribution of Calpains I and II in Rat Brain. *J. Neurosci.* **1986**, *6*, 3103−3111.

(11) Saatman, K. E.; Creed, J.; Raghupathi, R. Calpain as a Therapeutic Target in Traumatic Brain Injury. *Neurotherapeutics* **2010**, *7*, 31−42.

(12) Siman, R.; Giovannone, N.; Hanten, G.; Wilde, E. A.; McCauley, S. R.; Hunter, J. V.; Li, X.; Levin, H. S.; Smith, D. H. Evidence That the Blood Biomarker SNTF Predicts Brain Imaging Changes and Persistent Cognitive Dysfunction in Mild TBI Patients. *Front. Neurol.* **2013**, *4*, No. 190.

(13) Gan, Z. S.; Stein, S. C.; Swanson, R.; Guan, S.; Garcia, L.; Mehta, D.; Smith, D. H. Blood Biomarkers for Traumatic Brain Injury: A Quantitative Assessment of Diagnostic and Prognostic Accuracy. *Front. Neurol.* **2019**, *10*, No. 446.

(14) Kwong, G. A.; von Maltzahn, G.; Murugappan, G.; Abudayyeh, O.; Mo, S.; Papayannopoulos, I. A.; Sverdlov, D. Y.; Liu, S. B.; Warren, A. D.; Popov, Y.; et al. Mass-Encoded Synthetic Biomarkers for Multiplexed Urinary Monitoring of Disease. *Nat. Biotechnol.* **2013**, *31*, 63−70.

(15) Kwon, E. J.; Dudani, J. S.; Bhatia, S. N. Ultrasensitive Tumour-Penetrating Nanosensors of Protease Activity. *Nat. Biomed. Eng.* **2017**, *1*, No. 0054.

(16) Xiong, Y.; Mahmood, A.; Chopp, M. Animal Models of Traumatic Brain Injury. *Nat. Rev. Neurosci.* **2013**, *14*, 128−142.

(17) Hall, E. D.; Sullivan, P. G.; Gibson, T. R.; Pavel, K. M.; Thompson, B. M.; Scheff, S. W. Spatial and Temporal Characteristics of Neurodegeneration after Controlled Cortical Impact in Mice: More than a Focal Brain Injury. *J. Neurotrauma* **2005**, *22*, 252−265.

(18) Chen, Y. C.; Mao, H.; Yang, K. H.; Abel, T.; Meaney, D. F. A Modified Controlled Cortical Impact Technique to Model Mild Traumatic Brain Injury Mechanics in Mice. *Front. Neurol.* **2014**, *5*, No. 100.

(19) Pike, B. R.; Flint, J.; Dutta, S.; Johnson, E.; Wang, K. K. W.; Hayes, R. L. Accumulation of Non-Erythroid AII-Spectrin and Calpain-Cleaved AII-Spectrin Breakdown Products in Cerebrospinal Fluid after Traumatic Brain Injury in Rats. *J. Neurochem.* **2001**, *78*, 1297−1306.

(20) Saatman, K. E.; Bozyczko-Coyne, D.; Marcy, V.; Siman, R.; McIntosh, T. K. Prolonged Calpain-Mediated Spectrin Breakdown Occurs Regionally Following Experimental Brain Injury in the Rat. *J. Neuropathol. Exp. Neurol.* **1996**, *55*, 850−860.

(21) Zhao, X.; Posmantur, R.; Kampfl, A.; Liu, S.-J.; Wang, K. K. W.; Newcomb, J. K.; Pike, B. R.; Clifton, G. L.; Hayes, R. L. Subcellular Localization and Duration of μ-Calpain and m-Calpain Activity after Traumatic Brain Injury in the Rat: A Casein Zymography Study. *J. Cereb. Blood Flow Metab.* **1998**, *18*, 161−167.

(22) Ringger, N. C.; Tolentino, P. J.; McKinsey, D. M.; Pike, B. R.; Wang, K. K. W.; Hayes, R. L. Effects of Injury Severity on Regional and Temporal mRNA Expression Levels of Calpains and Caspases after Traumatic Brain Injury in Rats. *J. Neurotrauma* **2004**, *21*, 829−841.

(23) Price, L.; Wilson, C.; Grant, G. Blood−Brain Barrier Pathophysiology Following Traumatic Brain Injury. In *Translational Research in Traumatic Brain Injury*; Laskowitz, D.; Grant, G., Eds.; CRC Press/Taylor and Francis Group: Boca Raton, FL, 2016; pp 85−96.

(24) Hicks, R. R.; Baldwin, S. A.; Scheff, S. W. Serum Extravasation and Cytoskeletal Alterations Following Traumatic Brain Injury in Rats. *Mol. Chem. Neuropathol.* **1997**, *32*, 1−16.
(25) Kwon, E. J.; Skalak, M.; Lo Bu, R.; Bhatia, S. N. Neuron-Targeted Nanoparticle for siRNA Delivery to Traumatic Brain Injuries. *ACS Nano* **2016**, *10*, 7926−7933.
(26) Caliceti, P.; Veronese, F. M. Pharmacokinetic and Biodistribution Properties of Poly(Ethylene Glycol)−Protein Conjugates. *Adv. Drug Delivery Rev.* **2003**, *55*, 1261−1277.
(27) Boyd, B. J.; Galle, A.; Daglas, M.; Rosenfeld, J. V.; Medcalf, R. Traumatic Brain Injury Opens Blood−Brain Barrier to Stealth Liposomes via an Enhanced Permeability and Retention (EPR)-like Effect. *J. Drug Targeting* **2015**, *23*, 847−853.
(28) Bharadwaj, V. N.; Lifshitz, J.; Adelson, P. D.; Kodibagkar, V. D.; Stabenfeldt, S. E. Temporal Assessment of Nanoparticle Accumulation after Experimental Brain Injury: Effect of Particle Size. *Sci. Rep.* **2016**, *6*, No. 29988.
(29) Mitala, C. M.; Wang, Y.; Borland, L. M.; Jung, M.; Shand, S.; Watkins, S.; Weber, S. G.; Michael, A. C. Impact of Microdialysis Probes on Vasculature and Dopamine in the Rat Striatum: A Combined Fluorescence and Voltammetric Study. *J. Neurosci. Methods* **2008**, *174*, 177−185.
(30) Longmire, M.; Choyke, P. L.; Kobayashi, H. Clearance Properties of Nano-Sized Particles and Molecules as Imaging Agents: Considerations and Caveats. *Nanomedicine* **2008**, *3*, 703−717.
(31) Kwong, G. A.; Dudani, J. S.; Carrodeguas, E.; Mazumdar, E. V.; Zekavat, S. M.; Bhatia, S. N. Mathematical Framework for Activity-Based Cancer Biomarkers. *Proc. Natl. Acad. Sci. U.S.A.* **2015**, *112*, 12627−12632.
(32) Habgood, M. D.; Bye, N.; Dziegielewska, K. M.; Ek, C. J.; Lane, M. A.; Potter, A.; Morganti-Kossmann, C.; Saunders, N. R. Changes in Blood-Brain Barrier Permeability to Large and Small Molecules Following Traumatic Brain Injury in Mice. *Eur. J. Neurosci.* **2007**, *25*, 231−238.
(33) Stockholm, D.; Bartoli, M.; Sillon, G.; Bourg, N.; Davoust, J.; Richard, I. Imaging Calpain Protease Activity by Multiphoton FRET in Living Mice. *J. Mol. Biol.* **2005**, *346*, 215−222.
(34) Levesque, S.; Wilson, B.; Gregoria, V.; Thorpe, L. B.; Dallas, S.; Polikov, V. S.; Hong, J.-S.; Block, M. L. Reactive Microgliosis: Extracellular μ-Calpain and Microglia-Mediated Dopaminergic Neurotoxicity. *Brain* **2010**, *133*, 808−821.
(35) Thorek, D. L. J.; Watson, P. A.; Lee, S.-G.; Ku, A. T.; Bournazos, S.; Braun, K.; Kim, K.; Sjöström, K.; Doran, M. G.; Lamminmaki, U.; et al. Internalization of Secreted Antigen-Targeted Antibodies by the Neonatal Fc Receptor for Precision Imaging of the Androgen Receptor Axis. *Sci. Transl. Med.* **2016**, *8*, No. 367ra167.
(36) Urano, Y.; Sakabe, M.; Kosaka, N.; Ogawa, M.; Mitsunaga, M.; Asanuma, D.; Kamiya, M.; Young, M. R.; Nagano, T.; Choyke, P. L.; et al. Rapid Cancer Detection by Topically Spraying a γ-Glutamyltranspeptidase-Activated Fluorescent Probe. *Sci. Transl. Med.* **2011**, *3*, No. 110ra119.
(37) Whitley, M. J.; Cardona, D. M.; Lazarides, A. L.; Spasojevic, I.; Ferrer, J. M.; Cahill, J.; Lee, C.-L.; Snuderl, M.; Blazer, D. G., III; Hwang, E. S.; et al. A Mouse-Human Phase 1 Co-Clinical Trial of a Protease-Activated Fluorescent Probe for Imaging Cancer. *Sci. Transl. Med.* **2016**, *8*, No. 320ra4.
(38) Dudani, J. S.; Ibrahim, M.; Kirkpatrick, J.; Warren, A. D.; Bhatia, S. N. Classification of Prostate Cancer Using a Protease Activity Nanosensor Library. *Proc. Natl. Acad. Sci. U.S.A.* **2018**, *115*, 8954−8959.
(39) Guilfoyle, M. R.; Carpenter, K. L. H.; Helmy, A.; Pickard, J. D.; Menon, D. K.; Hutchinson, P. J. A. Matrix Metalloproteinase Expression in Contusional Traumatic Brain Injury: A Paired Microdialysis Study. *J. Neurotrauma* **2015**, *32*, 1553−1559.
(40) Costa, C.; Tortosa, R.; Domènech, A.; Vidal, E.; Pumarola, M.; Bassols, A. Mapping of Aggrecan, Hyaluronic Acid, Heparan Sulphate Proteoglycans and Aquaporin 4 in the Central Nervous System of the Mouse. *J. Chem. Neuroanat.* **2007**, *33*, 111−123.
(41) Mummert, M. E.; Mohamadzadeh, M.; Mummert, D. I.; Mizumoto, N.; Takashima, A. Development of a Peptide Inhibitor of Hyaluronan-Mediated Leukocyte Trafficking. *J. Exp. Med.* **2000**, *192*, 769−779.
(42) Mann, A. P.; Scodeller, P.; Hussain, S.; Joo, J.; Kwon, E.; Braun, G. B.; Mölder, T.; She, Z.-G.; Kotamraju, V. R.; Ranscht, B.; et al. A Peptide for Targeted, Systemic Delivery of Imaging and Therapeutic Compounds into Acute Brain Injuries. *Nat. Commun.* **2016**, *7*, No. 11980.

https://dx.doi.org/10.1021/acssensors.9b01812
ACS Sens. XXXX, XXX, XXX−XXX